Characterization and Application of Nanomaterials 2025, 8(1), 10521.
https://doi.org/10.24294/can10521

Article

Tuning dielectric properties in metal-doped NiO nanoparticles

Muhammad Fasih Aamir[1,2,3,*,†], Ahmar Ali[3,4,†], Kashif Nadeem[3]

[1] International Center for Materials Nanoarchitectonics (MANA), National Institute for Materials Science (NIMS), 1-1 Namiki, Tsukuba 305-0044, Japan
[2] Graduate School of Science and Technology, University of Tsukuba, 1-1-1 Tennodai, Tsukuba Ibaraki 305-8577, Japan
[3] Department of Physics, Faculty of Basic and Applied Sciences (FBAS), International Islamic University (IIU), Islamabad 44000, Pakistan
[4] King Fahd University of Petroleum and Minerals (KFUPM), Academic Belt Road, Dhahran 31261, Saudi Arabia
*** Corresponding authors:** Muhammad Fasih Aamir, AAMIR.MuhammadFasih@nims.go.jp
[†] These authors contributed equally to this work

CITATION

Aamir MF, Ali A, Nadeem K. Tuning dielectric properties in metal-doped NiO nanoparticles. Characterization and Application of Nanomaterials. 2025; 8(1): 10521. https://doi.org/10.24294/can10521

ARTICLE INFO

Received: 15 November 2024
Accepted: 23 December 2024
Available online: 15 January 2025

Abstract: Nickel Oxide (NiO) nanoparticles (NPs), doped with manganese (Mn) and cobalt (Co) at concentrations up to 8%, were synthesized using the composite hydroxide method (CHM). X-ray diffraction (XRD) analysis confirmed the formation of a cubic NiO structure, with no additional peaks detected, indicating successful doping. The average crystallite size was determined to range from 15 to 17.8 nm, depending on the dopant concentration. Scanning electron microscopy (SEM) images revealed mostly spherical, agglomerated particles, likely due to magnetic interactions. Fourier Transform Infrared Spectroscopy (FTIR) confirmed the incorporation of Mn and Co into the NiO lattice, consistent with the XRD results. The dielectric properties exhibited a high dielectric constant at low frequencies, which can be attributed to ion jump orientation and space charge effects. The imaginary part of the dielectric constant decreased with increasing frequency, as it became harder for electrons to align with the alternating field at higher frequencies. Both the real and imaginary dielectric constants showed behavior consistent with Koop's theory, increasing at low frequencies and decreasing at higher frequencies. Dielectric loss was primarily attributed to dipole flipping and charge migration. AC conductivity increased with frequency, and exhibited higher conductivity at high frequencies due to small polaron hopping. These co-doped NPs show potential for applications in solid oxide fuel cells.

Keywords: dielectrics; AC conductivity; koop's theory; space charge effect; metal doped nanoparticles

1. Introduction

Transition metal oxide nanoparticles, including materials such as nickel oxide (NiO), manganese oxide (MnO), iron oxide (FeO), and cobalt oxide (CoO), have garnered substantial interest due to their remarkable characteristics at the nanoscale [1–4]. These materials exhibit distinctive properties that diverge significantly from their bulk counterparts, influenced by factors such as particle size, surface effects, and electrical behavior [5–8]. Among them, NiO emerges as a particularly promising candidate, recognized for its role as a p-type semiconductor [9,10]. It exhibits a high exciton binding energy and a bandgap in the range of 3.6 to 4.0 eV, offering unique advantages over other metal oxides. NiO's antiferromagnetic nature, combined with its electrically insulating behavior and rock-salt cubic structure, further enhances its appeal [11]. These characteristics, alongside its chemical stability and suitability for diverse technological applications, have positioned NiO at the forefront of research in materials science [12,13].

Despite its many benefits, NiO's low conductivity at room temperature, with resistance on the order of 10^{13} Ω-cm, poses challenges for certain applications [14]. This behavior is linked to charge carrier hopping facilitated by Ni_2^+ vacancies, which limits its electrical performance. Modifying the material through doping offers a viable solution to this problem [15]. For instance, introducing monovalent elements like lithium generates Ni_3^+ ions, which effectively reduces resistivity [16]. However, while bulk and single-crystal forms of NiO have been widely studied, the dielectric behavior of NiO nanoparticles, particularly co-doped variants, remains underexplored [17]. This knowledge gap underscores the need for further investigation into how innovative doping strategies can unlock the full potential of NiO in practical applications [18,19].

The structural and compositional properties of NiO are intrinsically linked to its nanoscale behavior [20]. NiO adopts a rock-salt lattice configuration, with octahedral coordination of Ni_2^+ and O_2^- ions [21]. Its appearance is influenced by stoichiometry, transitioning from black in stoichiometric compositions to greenish hues when non-stoichiometric [22]. These optical and structural changes highlight the importance of controlling stoichiometry to optimize performance [23]. Additionally, factors such as synthesis method, particle size, annealing time, and doping significantly influence the properties of NiO at the nanoscale [24]. Managing structural and compositional defects, which are often intrinsic to nanostructured materials, is a critical challenge [25]. Addressing these defects is essential for enhancing the performance and reliability of NiO-based devices [26].

Defects within nanostructured materials play a pivotal role in shaping their electrical and dielectric properties [27,28]. For example, magnetic nanoparticles often experience strong interparticle interactions that lead to agglomeration, which can negatively impact material performance [29]. Single-doping strategies, while effective in introducing new functionalities, often result in clustering of the dopant within the host lattice, creating inhomogeneities. Co-doping presents a more sophisticated approach, addressing these limitations by introducing two dopant elements simultaneously [30]. This technique not only prevents dopant clustering but also enables fine-tuning of the material's electronic, magnetic, and dielectric properties. Co-doping has proven effective in enhancing conductivity, improving magnetic interactions, and achieving more uniform defect distributions [31].

The dielectric properties of NiO nanoparticles have been the focus of several studies. For instance, Different studies demonstrated the potential of NiO nanoparticles synthesized through wet chemical precipitation, reporting a large dielectric constant [32]. Similarly, some authors investigated NiO nanoparticles prepared via the sol-gel method and found that dielectric loss decreases with increasing frequency, attributed to the inability of ions to respond to alternating fields at higher frequencies [33,34]. These findings underscore the importance of dielectric studies in understanding and optimizing NiO for practical applications. However, there remains a significant gap in research on the frequency-dependent dielectric properties of co-doped NiO nanoparticles, providing a clear motivation for further exploration [35,36].

To address these challenges, this study investigates the effects of co-doping NiO nanoparticles with manganese (Mn) and cobalt (Co). These elements were chosen for

their ability to enhance both dielectric and magnetic properties while maintaining structural stability [37]. Co-doping introduces new energy states into the NiO lattice, facilitating charge carrier hopping and improving conductivity. Furthermore, the combination of Mn and Co ensures a more even distribution of dopant ions within the host matrix, minimizing the clustering observed in single-doped systems. This approach not only optimizes the dielectric response but also enhances the overall performance of the material.

The frequency-dependent dielectric behavior of NiO is particularly noteworthy. Dielectric properties, such as real and imaginary dielectric constants, exhibit distinct frequency-dependent trends [38]. At low frequencies, the dielectric constant is influenced by space charge effects and ion jump orientation, aligning with Koop's theory [39]. At higher frequencies, these effects diminish, resulting in a decrease in the dielectric constant as charge carriers are unable to keep pace with the alternating field [40]. By leveraging co-doping, this study aims to refine these properties, creating materials with tailored electrical and dielectric behavior for advanced applications [41,42].

The study also sheds light on the magnetic properties of co-doped NiO nanoparticles [43]. Mn and Co co-doping enhances magnetic interactions, reducing agglomeration caused by interparticle forces and improving the uniformity of particle dispersion [44]. These magnetic improvements, combined with enhanced dielectric performance, have significant implications for the use of co-doped NiO in applications such as solid oxide fuel cells [45–47]. The increased AC conductivity observed in co-doped NiO nanoparticles, particularly at higher frequencies, can be attributed to small polaron hopping, which further underscores their potential in energy-related technologies [48–50].

This research addresses critical challenges in the design of nanostructured materials, focusing on defect control and achieving optimal dopant distribution. By employing a co-doping strategy, the study demonstrates how the structural, electrical, and dielectric properties of materials can be simultaneously enhanced, offering a pathway to tailor these properties for specific functional requirements. Investigating the synthesis and frequency-dependent dielectric properties of both undoped and Mn-Co co-doped NiO nanoparticles, the research emphasizes their potential for superior performance. The novelty of this work lies in using the Composite Hydroxide Method (CHM), a simple and cost-effective approach that allows precise control over dopant concentration. By overcoming the challenges of defect management and dopant clustering in single-doped systems, this study contributes to creating materials with refined characteristics suitable for practical applications. The insights gained into the role of Mn and Co co-doping in enhancing dielectric performance, conductivity, and ion mobility in NiO nanoparticles pave the way for innovative applications in cutting-edge technologies, including renewable energy systems, high-performance electronics, solid oxide fuel cells, capacitors, and advanced sensors, offering new opportunities for technological advancements.

2. Experimental details

Composite Hydroxide Method (CHM) is a low-temperature method for

synthesizing single-phase nanoparticles (NPs). In this process, composite hydroxides are used as a solvent. It is a one-step process where all raw materials are mixed with hydroxides and placed in a beaker. The beaker is then placed in an oven at 200 ℃ for 24 h, allowing the NPs to form. After 24 h, the heating is stopped, and the sample is washed with distilled water to remove impurities. To form NiO NPs and Mn-Co co-doped NiO NPs, a specified number of mixed hydroxides (KOH, NaOH) is added to the beaker. Nickel nitrate is then combined with the hydroxides, and the mixture is placed in an oven at 200 ℃ for 24 h. Afterward, the sample is allowed to cool to room temperature. Finally, the sample is washed several times with distilled water to remove impurities, resulting in the desired NiO and co-doped NiO NPs. A flow chart illustrating the composite hydroxide-mediated method for preparing NiO and Mn-Co-doped NiO nanoparticles is shown in.

3. Results and discussions

3.1. X-ray diffraction

Figure 1a presents the XRD patterns of NiO and Mn-Co co-doped NiO nanoparticles with varying concentrations. The samples are labeled as S1 = undoped NiO, S2 = 2% Mn-6% Co doped NiO, S3 = 4% Mn-4% Co doped NiO, and S4 = 6% Mn-2% Co doped NiO. The diffraction peaks observed at 2θ = 37.30°, 43.30°, 62.90°, 75.30°, and 80.0° correspond to the (111), (200), (220), (311), and (222) crystal planes, respectively. These peaks align with JCPDS, No. 04-0835 data for NiO, confirming the formation of a cubic structure. The absence of additional peaks indicates high purity and successful doping, with no secondary phases detected.

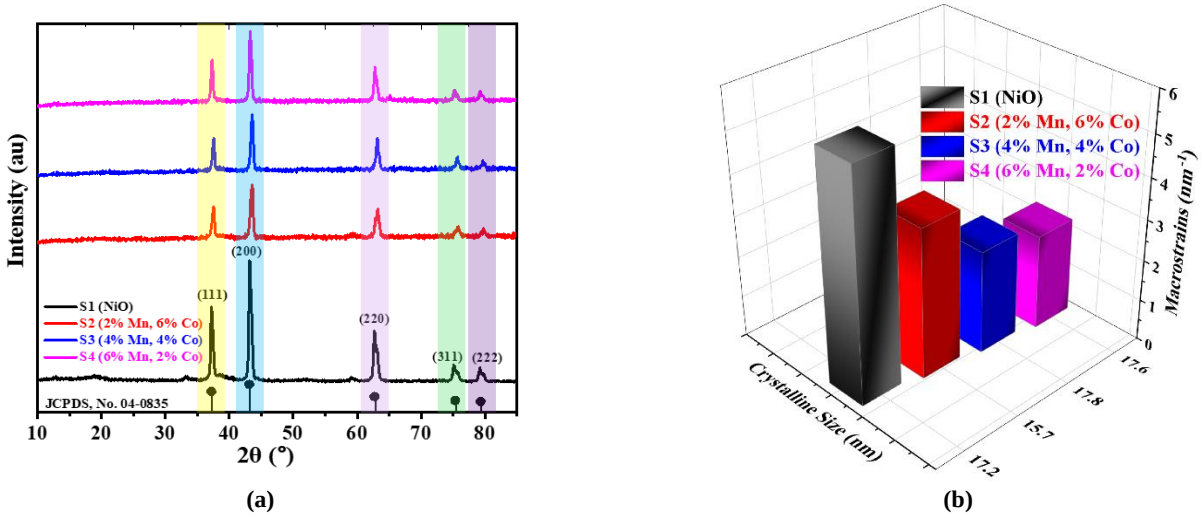

(a) **(b)**

Figure 1. (a) XRD pattern of NiO pure and co-doped NiO nanoparticles with JCPDS data; **(b)** Macrostrain vs crystalline size of NiO nanoparticles.

The crystallite size and lattice distortions varied with the dopant concentrations, as reflected by slight shifts in the diffraction peaks, which are attributed to differences in the ionic radii of Mn and Co. Furthermore, macrostrain was calculated for each crystal plane using the FWHM values and Bragg angles with the relation as:

$$\varepsilon = \frac{\beta}{4tan\delta}$$

where ε is the dielectric constant, β is the full width at half maximum (FWHM) and δ is Bragg angle [51]. The calculated macrostrain values were: (111) = 0.00660, (200) = 0.00561, (220) = 0.00367, (311) = 0.00253, and (222) = 0.00233. These results confirm the uniform incorporation of Mn and Co into the NiO lattice, with macrostrain progressively decreasing from the (111) to the (222) planes, further highlighting the influence of doping on the structural properties.

Macrostrain and crystallite effects in MN-CO doped NiO

Figure 1b illustrates the relationship between macrostrain and crystallite size, revealing the influence of Mn-Co doping concentrations on structural and dielectric properties of NiO. Macrostrain, calculated for different crystal planes using the FWHM values and Bragg angles, shows a progressive decrease from the (111) to the (222) planes, highlighting the uniform incorporation of dopants into the NiO lattice. This decreasing trend indicates reduced lattice distortions, which directly correlates with changes in crystallite size.

The observed variations in macrostrain and crystallite effects are significant for optimizing the dielectric properties of NiO. Higher macrostrain in the (111) and (200) planes correspond to greater lattice distortions, which can enhance polarization effects, improving the dielectric constant. Conversely, reduced macrostrain in the (220), (311), and (222) planes align with improved structural stability, facilitating the reduction of dielectric losses.

This interplay between macrostrain and crystallite size demonstrates the potential of Mn-Co doping to tailor the dielectric properties of NiO, making it suitable for advanced electronic and energy storage applications. The optimization of doping concentrations is critical to achieving the desired balance between dielectric constant and loss, as reflected in the graph.

3.2. Fourier transform infrared spectroscopy

Figure 2 presents the Fourier transform infrared spectroscopy (FTIR) spectra of both undoped and co-doped NiO nanoparticles, with varying concentrations of Mn and Co, within the wavenumber range of 350 to 1000 cm^{-1}. The prominent bands between 400 and 600 cm^{-1} are attributed to the stretching vibration mode of NiO, confirming the presence of NiO in all samples. This specific range is characteristic of Ni-O bond vibrations, indicating the formation of the NiO lattice structure. An absorption peak around 620 cm^{-1} further validates the presence of NiO, which is a typical feature in the FTIR spectra of nickel oxide. Additionally, a band observed at 870 cm^{-1} corresponds to the stretching and bending vibrations of C-O species, which are commonly present due to environmental exposure, such as carbon dioxide and moisture absorption from the air during synthesis and handling. This peak suggests that the nanoparticles may have adsorbed atmospheric contaminants or surface-bound species, which is typical in nanoparticle synthesis under ambient conditions.

Importantly, no additional peaks appear in the FTIR spectra of the Mn-Co co-doped NiO nanoparticles compared to the undoped NiO. This lack of extra peaks

indicates that the dopants (Mn and Co) are successfully integrated into the NiO lattice without forming separate phases or clusters. The absence of distinct peaks corresponding to Mn or Co oxides suggests that these dopants are likely dispersed or substituted within the NiO crystal structure, ensuring uniform doping. This behavior confirms a successful doping process where the metal ions (Mn^{2+} and Co^{2+}) replace Ni^{2+} ions in the lattice without causing significant structural disturbances. The findings highlight the effectiveness of the co-doping strategy in modifying NiO properties while maintaining its structural integrity, which is essential for applications in electronics, catalysis, and energy storage devices.

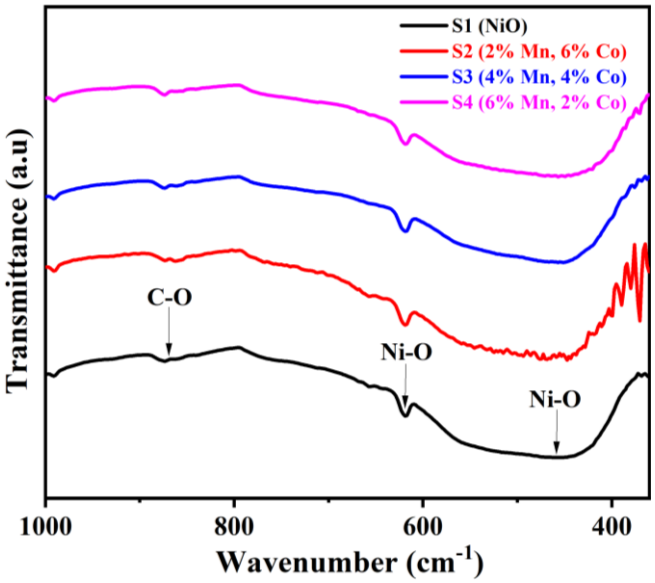

Figure 2. FTIR spectra of pure and co-doped NiO nanoparticles.

3.3. Scanning electron microscopy

Figure 3 displays the SEM (Scanning Electron Microscope) micrographs of undoped and Mn-Co co-doped NiO nanoparticles at a magnification of 30,000x. The images reveal that the synthesized nanoparticles predominantly exhibit a spherical morphology. However, the particles appear highly agglomerated, likely due to the magnetic interactions between the Mn and Co dopants within the NiO matrix. Such agglomeration is a common phenomenon in magnetic nanoparticles, as magnetic forces cause particle clustering, which can influence the material's properties. Despite this, the overall shape and distribution of the particles provide valuable insights into the effects of Mn-Co doping on the morphology of NiO nanoparticles.

Table 1. Structural parameters of NiO pure and co-doped NiO nanoparticles.

Samples	Planes (hkl)	2 Theta	FWHM (radians)	Lattice constant (A^0)	Average crystalline size D (nm)	Dislocation density $\delta = 1/D^2$ $1/nm^2$
Un-doped NiO	200	43.27	0.5106	0.208	17.2	0.0029
S2	200	43.29	0.5139	0.207	15.7	0.0029
S3	200	43.55	0.4481	0.207	17.8	0.0022
S4	200	43.30	0.4488	0.208	17.6	0.0022

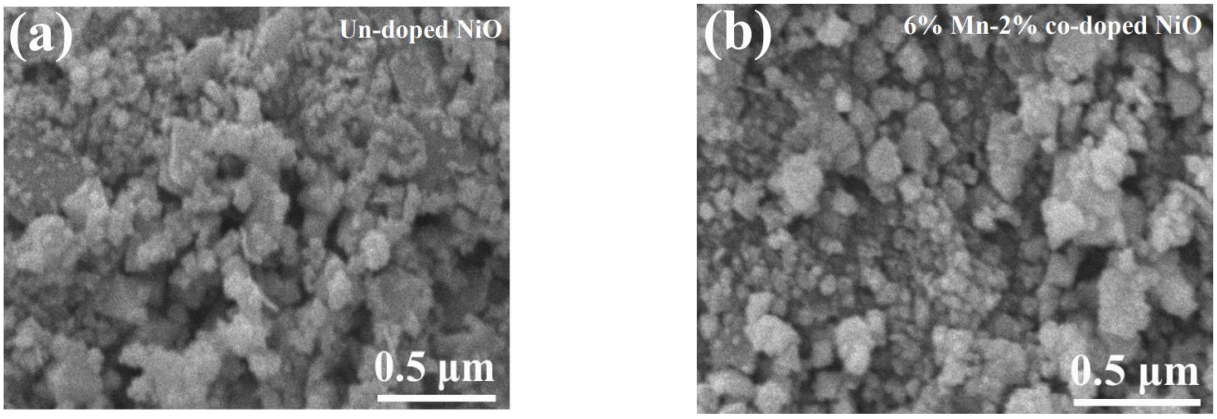

(a) **(b)**

Figure 3. SEM images of co-doped NiO nanoparticles **(a)** Undoped NiO; **(b)** Doped NiO.

3.4. Dielectric properties

The dielectric properties of nanoparticles are influenced by various factors, including the synthesis method, grain size, annealing temperature, and AC conductivity. In the case of NiO and its Mn, Co co-doped derivatives, the crystallite size plays a crucial role in shaping the dielectric behavior as shown in **Table 1**. Smaller crystallites typically result in higher dielectric constants at low frequencies, as the material exhibits enhanced ion jump orientation and space charge effects. As the crystallite size increases, the material's AC conductivity tends to improve, which in turn influences the dielectric loss and behavior at higher frequencies. These observations highlight that crystallite size is a key parameter in tailoring the dielectric properties of NiO-based materials for applications in electronic devices and energy storage systems. In this study, dielectric measurements were conducted on pure NiO and Mn, Co co-doped NiO samples, exploring their frequency-dependent dielectric constants and loss over a range of dopant concentrations and frequencies from 1 kHz to 2 MHz.

3.4.1. Frequency vs real part

The dielectric constant is calculated by using the relation [52],

$$\varepsilon_r = \frac{Cd}{\varepsilon_0 A}$$

where;

ε_r is the relative permittivity (dielectric constant) of the material,

C is the measured capacitance of the material,

d is the thickness of the material,

ε_0 is the vacuum permittivity (approximately 8.854×10^{-12} F/m),

A is the area of the electrodes.

Figure 4a shows that at low frequencies, the dielectric constant increases, and at higher frequencies, it decreases. The higher value of the dielectric constant at low frequency may be attributed to the increased ion jump orientation effect and the enhanced space charge effect exhibited by the nanoparticles. In nanocrystalline materials, most of the atoms reside at the grain boundaries, where they become

electrically active due to charge trapping. The changes in the electric field can be easily followed by the dipole moment at low frequencies. As a result, space charge polarization and rotational polarization occur at the interfaces, enhancing the dielectric constant at low frequencies. These findings align with Koop's theory, which suggests that the grains are conductive, while the grain boundaries act as insulators. At higher frequencies, it becomes more difficult for electrons to align with the alternating electric field, causing the dielectric constant to decrease. NiO nanoparticles with co-doping of Mn and Co show a higher dielectric constant at low frequencies compared to pure NiO, due to the larger polarization in the co-doped nanoparticles.

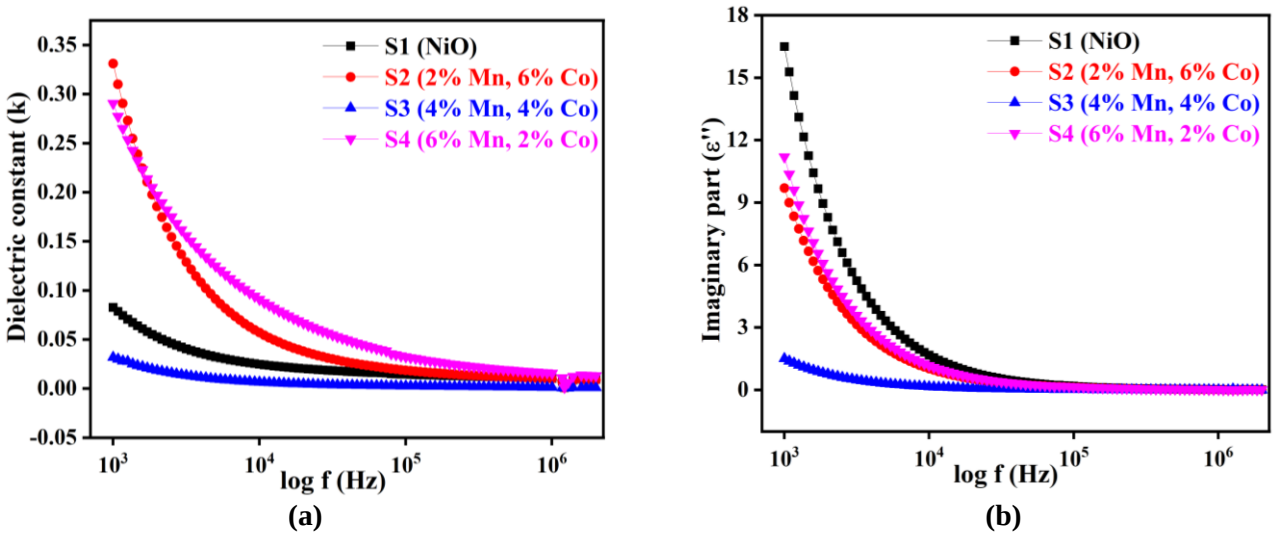

Figure 4. (a) Dielectric constant of NiO nanoparticles; **(b)** Imaginary part of NiO nanoparticles.

3.4.2. Frequency vs imaginary part

Figure 4b represents the frequency dependence of the imaginary part of the dielectric constant. The imaginary part of the dielectric constant reflects the energy loss within the material when it is subjected to an alternating electric field. It indicates the resistance offered by the material to the applied electric field and provides insights into the material's ability to store and dissipate energy. For an ideal, pure dielectric material, the imaginary part of the dielectric constant would be zero, as there would be no energy dissipation. However, in practical materials, the imaginary part is non-zero and varies with frequency. This part is calculated using the formula [53];

$$\varepsilon'' = \varepsilon' tan\ \delta$$

where;

ε'' is the imaginary part of the dielectric constant, which corresponds to the energy loss in the material.

ε' is the real part of the dielectric constant, which represents the energy stored in the material.

tan δ is the loss tangent, a measure of the energy dissipation in the material when it is exposed to an alternating electric field. It is defined as the ratio of the imaginary part to the real part of the dielectric constant.

As the frequency increases, the imaginary part of the dielectric constant typically

decreases. This occurs because, at higher frequencies, the electrons within the material struggle to keep up with the rapidly alternating field, making it harder for them to align with the field direction. As a result, the energy loss due to electron alignment decreases with increasing frequency, causing the imaginary part of the dielectric constant to reduce. This frequency-dependent behavior is essential in understanding how the material performs under different operating conditions, particularly in applications like capacitors, sensors, and energy storage devices.

3.4.3. Frequency vs tangent loss

Figure 5 shows the frequency dependence of the tangent loss for NiO, also known as the dissipation factor. Mathematically, it can be expressed as [54]:

$$tan\ \delta = \varepsilon''/\varepsilon'$$

The dielectric loss tangent is higher at low frequencies and exhibits a decreasing trend at higher frequencies. This decrease in the dissipation factor follows Koop's model. Dielectric loss primarily results from the flipping of dipoles and the migration of charge carriers from the grains to the grain boundaries. At low frequencies, the grain boundaries are more dominant and provide more resistance to the flow of electrons, resulting in a higher tangent loss in this region. Undoped NiO has a larger tangent loss compared to co-doped nanomaterials, likely due to the larger imaginary part of undoped NiO at low frequencies, which may be attributed to its smaller particle size compared to other samples.

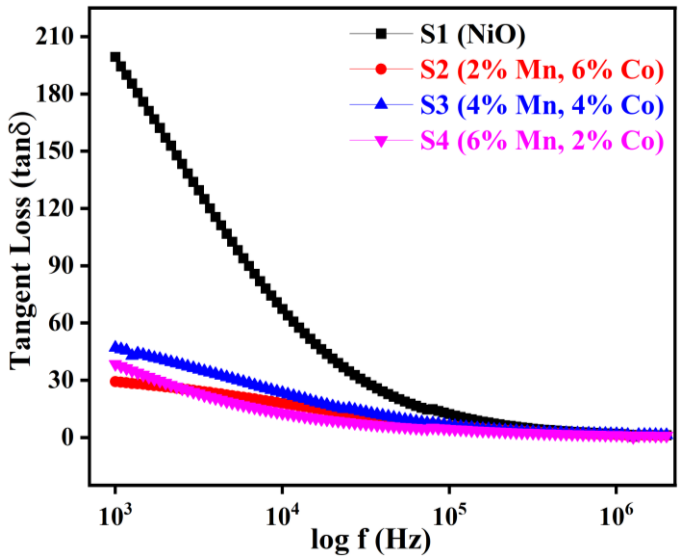

Figure 5. Frequency dependence for tangent loss for NiO nanoparticles.

3.4.4. Frequency vs AC conductivity

AC conductivity illustrates about the conduction mechanism. We calculated it by using formula [55];

$$\sigma ac = \varepsilon' tan(\delta)\omega\varepsilon_0$$

where ac is the AC conductivity, which measures how well a material conducts electricity when subjected to an alternating electric field and ω: The angular frequency of the applied alternating field, defined as $\omega = 2\pi f$, where f is the frequency.

Figure 6 shows the frequency dependence of AC conductivity at room temperature for different concentrations of Mn and Co doped in NiO NPs. It is evident from the figure that all the samples exhibit an increase in conductivity with an increase in frequency. At low frequencies, the grain boundaries contribute significantly, making it difficult for electrons to overcome the barrier, leading to a minimum in AC conductivity. However, at higher frequencies, the role of the grains becomes more dominant, allowing electrons to move more easily, which results in a slight increase in AC conductivity compared to low frequencies. The conductivity of sample S4 is greater than that of the others, which may be due to the larger size of these co-doped NPs compared to S1, S2, and S3 samples. Additionally, the stronger small polaron hopping conduction mechanism in sample S4 may also contribute to this higher conductivity. These results suggest that the dielectric properties of co-doped NiO nanoparticles are strongly influenced by the nature of the dopants, their concentrations, and the average crystallite size of the NPs. These properties make them suitable for applications in energy conversion devices, such as solid oxide fuel cells.

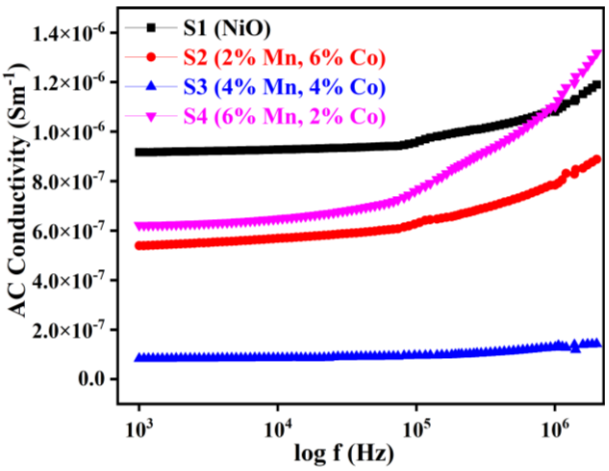

Figure 6. AC conductivity of pure and co-doped NiO nanoparticles.

4. Conclusions

NiO nanoparticles doped with varying concentrations of Mn and Co were successfully synthesized using the Composite Hydroxide Method (CHM). X-ray diffraction analysis confirmed the formation of a cubic crystal structure, consistent with the expected phase. Scanning Electron Microscopy (SEM) images revealed agglomeration of nanoparticles, likely caused by the magnetic interactions between the Mn and Co dopants within the NiO matrix. Fourier Transform Infrared Spectroscopy (FTIR) analysis further validated the successful co-doping of Mn and Co into the NiO structure. The observed high dielectric constant at low frequencies is attributed to enhanced ion jump orientation and space charge effects, while the imaginary dielectric constant decreased at higher frequencies, suggesting a difficulty in electron alignment with the alternating field. AC conductivity measurements revealed an increase in conductivity with frequency, influenced by both the grains and grain boundaries. Notably, S4 = 6% Mn-2% Co doped NiO exhibited the highest conductivity at higher frequencies, potentially due to the small polaron hopping

conduction mechanism and the increased crystallite size of the co-doped nanoparticles.

Author contributions: Conceptualization, MFA; methodology, MFA, AA and KN; validation, KN; formal analysis, MFA; investigation, MFA, AA and KN; resources, KN; data curation, MFA and KN; writing—original draft preparation, MFA and AA; writing—review and editing, MFA. All authors have read and agreed to the published version of the manuscript.

Conflict of interest: The authors declare no conflict of interest.

References

1. Rajenimbalkar RS, Deshmukh VJ, Patankar KK, et al. Effect of multivalent ion doping on magnetic, electrical, and dielectric properties of nickel ferrite nanoparticles. Scientific Reports. 2024; 14(1): 29547. doi: 10.1038/s41598-024-81222-3
2. Miroshnichenko AE, Evlyukhin AB, Yu YF, et al. Nonradiating anapole modes in dielectric nanoparticles. Nature Communications. 2015; 6(1): 8069. doi: 10.1038/ncomms9069
3. Yang Y, Gao P, Li L, et al. Electrochemical dynamics of nanoscale metallic inclusions in dielectrics. Nature Communications. 2014; 5(1): 4232. doi: 10.1038/ncomms5232
4. Jahani S, Jacob Z. All-dielectric metamaterials. Nature Nanotechnology. 2016; 11(1): 23–36. doi: 10.1038/nnano.2015.304
5. Li X, He S, Jiang Y, et al. Unraveling bilayer interfacial features and their effects in polar polymer nanocomposites. Nature Communications. 2023; 14(1): 5707. doi: 10.1038/s41467-023-41479-0
6. Sharma V, Wang C, Lorenzini RG, et al. Rational design of all organic polymer dielectrics. Nature Communications. 2014; 5(1): 4845. doi: 10.1038/ncomms5845
7. Khan AA, Mathur A, Yin L, et al. Breaking dielectric dilemma via polymer functionalized perovskite piezocomposite with large current density output. Nature Communications. 2024; 15(1). doi: 10.1038/s41467-024-53846-6
8. Sagadevan S, Pal K, Chowdhury ZZ, et al. Structural, optical and dielectric investigation of CdFe2O4nanoparticles. Materials Research Express. 2017; 4(7): 075025. doi: 10.1088/2053-1591/aa77b5
9. Lin Z, Du C, Yan B, et al. Two-dimensional amorphous NiO as a plasmonic photocatalyst for solar H2 evolution. Nature Communications. 2018; 9(1): 4036. doi: 10.1038/s41467-018-06456-y
10. Ahmad S, Usman M, Hashim M, et al. Investigation of Optical and Dielectric Properties of Nickel-Doped Zinc Oxide Nanostructures Prepared via Coprecipitation Method. Lovergine N, ed. Nanomaterials and Nanotechnology. 2024; 2024: 1–11. doi: 10.1155/2024/8330886
11. Sharma V, Chotia C, Tarachand T, et al. Influence of particle size and dielectric environment on the dispersion behaviour and surface plasmon in nickel nanoparticles. Physical Chemistry Chemical Physics. 2017; 19(21): 14096–14106. doi: 10.1039/c7cp01769c
12. Thongbai P, Tangwancharoen S, Yamwong T, et al. Dielectric relaxation and dielectric response mechanism in (Li, Ti)-doped NiO ceramics. Journal of Physics: Condensed Matter. 2008; 20(39): 395227. doi: 10.1088/0953-8984/20/39/395227
13. Hajalilou A, Kamari HM, Shameli K. Dielectric and electrical characteristics of mechanically synthesized Ni-Zn ferrite nanoparticles. Journal of Alloys and Compounds. 2017; 708: 813–826. doi: 10.1016/j.jallcom.2017.03.030
14. Sharma A, Hickman J, Gazit N, et al. Nickel nanoparticles set a new record of strength. Nature Communications. 2018; 9(1). doi: 10.1038/s41467-018-06575-6
15. Gong M, Zhou W, Tsai MC, et al. Nanoscale nickel oxide/nickel heterostructures for active hydrogen evolution electrocatalysis. Nature Communications. 2014; 5(1): 4695. doi: 10.1038/ncomms5695
16. Cheng S, Sheng D, Mukherjee S, et al. Carbon nanolayer-mounted single metal sites enable dipole polarization loss under electromagnetic field. Nature Communications. 2024; 15(1): 9077. doi: 10.1038/s41467-024-53465-1
17. Singh S, Verma R, Kaul N, et al. Surface plasmon-enhanced photo-driven CO2 hydrogenation by hydroxy-terminated nickel nitride nanosheets. Nature Communications. 2023; 14(1): 2551. doi: 10.1038/s41467-023-38235-9
18. Wang H, Liang Y, Gong M, et al. An ultrafast nickel–iron battery from strongly coupled inorganic nanoparticle/nanocarbon hybrid materials. Nature Communications. 2012; 3(1): 917. doi: 10.1038/ncomms1921

19. Neagu D, Oh TS, Miller DN, et al. Nano-socketed nickel particles with enhanced coking resistance grown in situ by redox exsolution. Nature Communications. 2015; 6(1): 8120. doi: 10.1038/ncomms9120
20. Suryanto BHR, Wang Y, Hocking RK, et al. Overall electrochemical splitting of water at the heterogeneous interface of nickel and iron oxide. Nature Communications. 2019; 10(1): 5599. doi: 10.1038/s41467-019-13415-8
21. Li HB, Yu MH, Wang FX, et al. Amorphous nickel hydroxide nanospheres with ultrahigh capacitance and energy density as electrochemical pseudocapacitor materials. Nature Communications. 2013; 4(1): 1894. doi: 10.1038/ncomms2932
22. Fan L, Liu PF, Yan X, et al. Atomically isolated nickel species anchored on graphitized carbon for efficient hydrogen evolution electrocatalysis. Nature Communications. 2016; 7(1):10667. doi: 10.1038/ncomms10667
23. Wang H, Lee HW, Deng Y, et al. Bifunctional non-noble metal oxide nanoparticle electrocatalysts through lithium-induced conversion for overall water splitting. Nature Communications. 2015; 6(1): 7261. doi: 10.1038/ncomms8261
24. Yun G, Tang SY, Sun S, et al. Liquid metal-filled magnetorheological elastomer with positive piezoconductivity. Nature Communications. 2019; 10(1): 1300. doi: 10.1038/s41467-019-09325-4
25. Zhou H, Yu F, Huang Y, et al. Efficient hydrogen evolution by ternary molybdenum sulfoselenide particles on self-standing porous nickel diselenide foam. Nature Communications. 2016; 7(1): 12765. doi: 10.1038/ncomms12765
26. Ali S, Khalid M, Nazir G, et al. Effect of nickel substitution on structural and dielectric properties of Mg-Zn based spinel ferrite nanoparticles. Physica Scripta. 2022; 97(6): 065802. doi: 10.1088/1402-4896/ac690f
27. Jiang J, Zhu J, Ai W, et al. Encapsulation of sulfur with thin-layered nickel-based hydroxides for long-cyclic lithium–sulfur cells. Nature Communications. 2015; 6(1): 8622. doi: 10.1038/ncomms9622
28. Qiu H, Xu T, Wang Z, et al. Hopping transport through defect-induced localized states in molybdenum disulphide. Nature Communications. 2013; 4(1): 2642. doi: 10.1038/ncomms3642
29. Kobayashi N, Masumoto H, Takahashi S, et al. Giant dielectric and magnetoelectric responses in insulating nanogranular films at room temperature. Nature Communications. 2014; 5(1): 4417. doi: 10.1038/ncomms5417
30. Rehman AU, Atif M, Rehman U ur, et al. Tuning the magnetic and dielectric properties of Fe3O4 nanoparticles for EMI shielding applications by doping a small amount of Ni2+/Zn2+. Materials Today Communications. 2023; 34: 105454. doi: 10.1016/j.mtcomm.2023.105454
31. Deonikar VG, Kulkarni VD, Rathod SM, et al. Fabrication and characterizations of structurally engineered lanthanum substituted nickel-cobalt ferrites for the analysis of electric and dielectric properties. Inorganic Chemistry Communications. 2020; 119: 108074. doi: 10.1016/j.inoche.2020.108074
32. Narender SS, Varma VVS, Srikar CS, et al. Nickel Oxide Nanoparticles: A Brief Review of Their Synthesis, Characterization, and Applications. Chemical Engineering & Technology. 2022; 45(3): 397–409. doi: 10.1002/ceat.202100442
33. Imran Din M, Rani A. Recent Advances in the Synthesis and Stabilization of Nickel and Nickel Oxide Nanoparticles: A Green Adeptness. International Journal of Analytical Chemistry. 2016; 2016: 1–14. doi: 10.1155/2016/3512145
34. Aamir MF, Mumtaz M, Saqib I, et al. Temperature driven shifts of super-conductance in Zn-doped CuTl-1223 nanoparticle. Journal of Materials Science: Materials in Electronics. 2024; 35(33): 1–12. doi: 10.1007/s10854-024-13848-y
35. Li Y, Fang L, Liu L, et al. Giant dielectric response and charge compensation of Li- and Co-doped NiO ceramics. Materials Science and Engineering: B. 2012; 177(9): 673–677. doi: 10.1016/j.mseb.2012.03.054
36. Dakhel AA. Dielectric relaxation behaviour of Li and La co-doped NiO ceramics. Ceramics International. 2013; 39(4): 4263–4268. doi: 10.1016/j.ceramint.2012.10.278
37. Manna S, De SK. Giant dielectric permittivity observed in Li and Zr co-doped NiO. Solid State Communications. 2010; 150(9–10): 399–404. doi: 10.1016/j.ssc.2009.11.044
38. Abdallah AM, Noun M, Awad R. Dielectric, impedance and conductivity properties of pristine and (Gd, Ru)-dual doped NiO nanoparticles. Journal of Alloys and Compounds. 2022; 910: 164952. doi: 10.1016/j.jallcom.2022.164952
39. Shaikh A, Bellad S, Chougule B. Temperature and frequency-dependent dielectric properties of Zn substituted Li–Mg ferrites. Journal of magnetism and magnetic materials. 1999; 195(2): 384–390.
40. Bhunia AK, Pradhan SS, Bhunia K, et al. Study of the optical properties and frequency-dependent electrical modulus spectrum to the analysis of electric relaxation and conductivity effect in zinc oxide nanoparticles. Journal of Materials Science: Materials in Electronics. 2021; 32(17): 22561–22578. doi: 10.1007/s10854-021-06742-4
41. Kaur J, Gupta V, Kotnala R, et al. Size dependent dielectric properties of Co and Fe doped SnO 2 nanoparticles and their nanorods by Ce co-doping. Materials Science, Physics; 2012.

42. Yücedağ İ, Kaya A, Altındal Ş. On the frequency dependent negative dielectric constant behavior in Al/Co-doped (PVC+TCNQ)/p-Si structures. International Journal of Modern Physics B. 2014; 28(23): 1450153. doi: 10.1142/s0217979214501537
43. Bharathy G, Raji P. Pseudocapacitance of Co doped NiO nanoparticles and its room temperature ferromagnetic behavior. Physica B: Condensed Matter. 2018; 530: 75–81. doi: 10.1016/j.physb.2017.10.106
44. Jothibas M, Bharanidharan K, Paulson E, et al. Effect of co-dopant proportion on the structural, optical and magnetic properties of pristine NiO nanoparticles synthesized by Sol–gel method. Journal of Materials Science: Materials in Electronics. 2022; 33: 907–919.
45. Rahman NU, Khan WU, Khan S, et al. A promising europium-based down conversion material: organic–inorganic perovskite solar cells with high photovoltaic performance and UV-light stability. Journal of Materials Chemistry A. 2019; 7(11): 6467–6474. doi: 10.1039/c9ta00551j
46. Rahman NU, Khan WU, Li W, et al. Simultaneous enhancement in performance and UV-light stability of organic–inorganic perovskite solar cells using a samarium-based down conversion material. Journal of Materials Chemistry A. 2019; 7(1): 322–329. doi: 10.1039/c8ta09362h
47. Shakoor A, Aman Nowsherwan G, Fasih Aamir M, et al. Performance Evaluation of Solar Cells by Different Simulating Softwares. Solar PV Panels—Recent Advances and Future Prospects; 2023.
48. Gallo AB, Simões-Moreira JR, Costa HKM, et al. Energy storage in the energy transition context: A technology review. Renewable and Sustainable Energy Reviews. 2016; 65: 800–822. doi: 10.1016/j.rser.2016.07.028
49. Waqas M, Shakoor A, Nadeem M, et al. Unveiling transport properties in rare-earth-substituted nanostructured bismuth telluride for thermoelectric application. Zeitschrift für Naturforschung A. 2023; 78(11): 1069–1080. doi: 10.1515/zna-2023-0162
50. Long Y, Xian Y, Yuan S, et al. π-π conjugate structure enabling the channel construction of carrier-facilitated transport in 1D–3D multidimensional CsPbI2Br solar cells with high stability. Nano Energy. 2021; 89: 106340. doi: 10.1016/j.nanoen.2021.106340
51. Takashima S, Schwan HP. Dielectric Dispersion of Crystalline Powders of Amino Acids, Peptides, and Proteins1. The Journal of Physical Chemistry. 1965; 69(12): 4176–4182. doi: 10.1021/j100782a019
52. Ishii K, Kinoshita M, Kuroda H. Dielectric Constant Measurement on Organic Crystalline Powder. Bulletin of the Chemical Society of Japan. 1973; 46(11): 3385–3391. doi: 10.1246/bcsj.46.3385
53. Aly K. Adjusting the relation between the imaginary part of the dielectric constant and the wavelength. Physica B: Condensed Matter. 2023; 655: 414723. doi: 10.1016/j.physb.2023.414723
54. Murtanto TB, Natori S, Nakamura J, et al. ac conductivity and dielectric constant of conductor-insulator composites. Physical Review B. 2006; 74(11). doi: 10.1103/physrevb.74.115206
55. Hill R, Jonscher A. DC and AC conductivity in hopping electronic systems. Journal of Non-Crystalline Solids. 1979; 32(1–3): 53–69.